

INCREASING BLACKHOLE FEEDBACK INDUCED QUENCHING WITH ANISOTROPIC THERMAL CONDUCTION

RAHUL KANNAN¹, MARK VOGELSBERGER^{1,6}, CHRISTOPH PFROMMER², RAINER WEINBERGER²
VOLKER SPRINGEL^{2,3}, LARS HERNQUIST⁴, EWALD PUCHWEIN⁵, RÜDIGER PAKMOR²

Draft version July 31, 2018

ABSTRACT

Feedback from central supermassive blackholes is often invoked to explain the low star formation rates in massive galaxies at the centers of galaxy clusters. However, the detailed physics of the coupling of the injected feedback energy with the intracluster medium is still unclear. Using high-resolution magnetohydrodynamic cosmological simulations of galaxy cluster formation, we investigate the role of anisotropic thermal conduction in shaping the thermodynamic structure of clusters, and, in particular, in modifying the impact of black hole feedback. Stratified anisotropically conducting plasmas are formally always unstable, and thus more prone to mixing, an expectation borne out by our results. The increased mixing efficiently isotropizes the injected feedback energy which in turn significantly improves the coupling between the feedback energy and the intracluster medium. This facilitates an earlier disruption of the cool core, reduces the star formation rate by more than an order of magnitude, and results in earlier quenching despite an overall lower amount of feedback energy injected into the cluster core. With conduction, the metallicity gradients and dispersions are lowered, aligning them better with observational constraints. These results highlight the important role of thermal conduction in establishing and maintaining quiescence of massive galaxies.

Subject headings: plasmas — conduction — magnetic fields — turbulence — instabilities — methods: numerical

1. INTRODUCTION

Feedback from active galactic nuclei (AGN) has widely been invoked to explain the quenching and quiescence of massive galaxies (Croton et al. 2006; Sijacki et al. 2007; Booth & Schaye 2009; Choi et al. 2012; Li & Bryan 2014; Weinberger et al. 2016). However, the details of how this feedback energy couples to the surrounding gas are still not properly understood, so the modelling efforts have been necessarily crude. Despite this limitation, recent cosmological models have had reasonable success in regulating the properties of massive central galaxies (e.g. Genel et al. 2014; Vogelsberger et al. 2014a; Schaye et al. 2015; Sijacki et al. 2015; Weinberger et al. 2016).

However, these galaxy formation simulations did not account for important physical processes related to thermal conduction and magnetic fields, which can significantly affect the properties of the intracluster medium (ICM) (Balbus 2000; Carilli & Taylor 2002; Quataert 2008). Thermal conduction has been conjectured to compensate for the cooling losses in the centers of clusters (Zakamska & Narayan 2003; Voit et al. 2015), but it is unclear if the actual amount of heat flow can be as high as expected from traditional theoretical estimates. For example, mirror instabilities and oblique whistler modes can potentially suppress electron transport (Komarov et al. 2016;

Riquelme et al. 2016; Roberg-Clark et al. 2016). However, the effective volume filling factor of these processes has not been studied. It is thus still unclear whether a corresponding suppression of the electron transport reduces the classical value of the conductivity significantly, especially in the presence of other mobile anisotropic particle distributions such as cosmic rays.

Recent simulations (Ruszkowski et al. 2011; Yang & Reynolds 2016) have shown that thermal conduction alone is not strong enough to offset the cooling losses even if a full Spitzer conduction coefficient along magnetic field lines is assumed. It may, however, provide part of the heating, reducing the burden on the blackhole (Yang & Reynolds 2016). It has also been found to enhance the mixing of the thermal plasma in the presence of external sources of turbulence like cosmic ray driven instabilities (Sharma et al. 2009; Banerjee & Sharma 2014).

In this Letter, we discuss high-resolution simulations of the formation of a galaxy cluster, with and without anisotropic thermal conduction. We investigate the interaction between AGN feedback, magnetic fields and anisotropic thermal conduction on both the integrated and small scale properties of the cluster. Our methodology is introduced in Section 2, the main results are presented in Section 3 and interpreted in Section 4, and finally, our conclusions are given in Section 5.

2. SIMULATIONS

We have carried out zoom-in cosmological simulations of a massive ($M_{200} \sim 6.5 \times 10^{14} M_{\odot}$) galaxy cluster as part of the AESTUS project (Kannan et al. in prep). The initial conditions for this cluster were generated from the Millennium XXL simulation (Angulo et al. 2012) and then rescaled to the latest Wilkinson Microwave Anisotropy Probe (WMAP)-9 measurements (Hinshaw et al. 2013): $\Omega_m = 0.2726$, $\Omega_{\Lambda} = 0.7274$, $\Omega_b = 0.0456$, $\sigma_8 = 0.809$, $n_s = 0.963$, and $H_0 = 100 h \text{ km s}^{-1} \text{ Mpc}^{-1}$ with $h = 0.704$. The high resolution dark matter (DM) and gas masses are $6.8 \times 10^7 M_{\odot}$

kannanr@mit.edu

¹ Department of Physics, Kavli Institute for Astrophysics & Space Research, Massachusetts Institute of Technology, Cambridge 02139, MA, USA

² Heidelberg Institute for Theoretical Studies, Schloss-Wolfsbrunnengasse 35, D-69118 Heidelberg, Germany

³ Zentrum für Astronomie der Universität Heidelberg, ARI, Mönchhofstr. 12-14, D-69120 Heidelberg, Germany

⁴ Harvard-Smithsonian Center for Astrophysics, 60 Garden Street, Cambridge, MA 02138, USA

⁵ Institute of Astronomy and Kavli Institute for Cosmology, University of Cambridge, Madingley Road, Cambridge, CB3 0HA, UK

⁶ Alfred P. Sloan Fellow

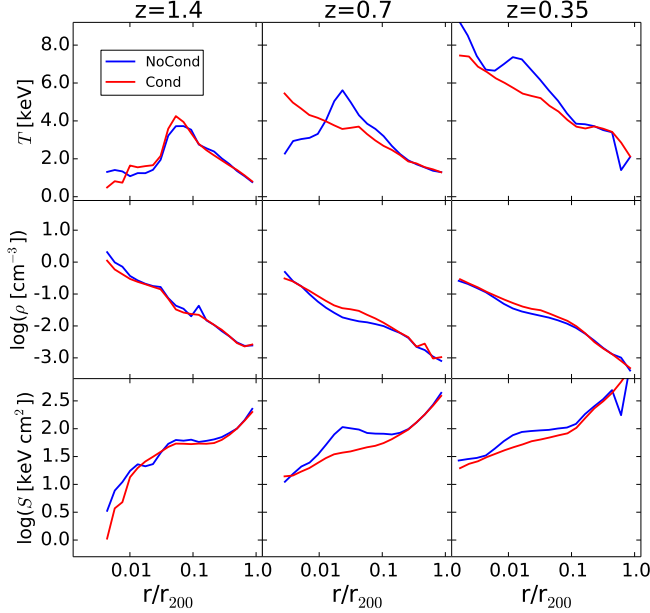


Figure 1. Temperature (T ; top row), density (ρ ; middle row) and entropy (S ; bottom row) profiles of the simulated cluster at three representative redshifts, $z = 1.4$ (left column), $z = 0.7$ (middle column) and $z = 0.35$ (right column) in the NoCond (blue curves) and Cond (red curves) runs.

and $1.1 \times 10^7 M_{\odot}$, respectively, with a softening length of 1.4 kpc for both particle types. Our mass resolution is ~ 1000 times and our spatial resolution ~ 30 times better than previous simulations attempting to model anisotropic thermal conduction in a cosmological context (Ruszkowski et al. 2011). We also achieve better resolution than idealized non-cosmological simulations with thermal conduction (Ruszkowski & Oh 2010; Parrish et al. 2012; Yang & Reynolds 2016) and recent cosmological pure hydrodynamic simulations of clusters (Hahn et al. 2015; Rasia et al. 2015).

The simulations were performed with the moving-mesh code AREPO (Springel 2010), using a module for ideal magnetohydrodynamics (MHD) (Pakmor & Springel 2013). The simulations employ a galaxy formation physics model originally developed for the ILLUSTRIS simulation suite (Vogelsberger et al. 2012, 2013, 2014a,b), updated with a new AGN feedback scheme (Weinberger et al. 2016) and modifications to the stellar wind scheme (Pillepich et al., in prep).

One of the runs (Cond) additionally includes anisotropic thermal conduction using the newly developed numerical approach introduced in Kannan et al. (2016). The value of the conduction coefficient is set to the canonical Spitzer value (Spitzer 1962) along the magnetic field, with a maximum value of the diffusivity ($\chi \sim \kappa/C_v\rho$) set to $5 \times 10^{31} \text{ cm}^2/\text{s}$ (Ruszkowski et al. 2011; Yang & Reynolds 2016) and zero in the perpendicular direction. The conduction routine is not active for star forming gas cells that follow an equation of state model for the star-forming interstellar medium (Springel & Hernquist 2003). The run without conduction is called NoCond in the following.

3. RESULTS

Fig. 1 shows the temperature (top row), density (middle row) and entropy (bottom row) profiles for both the NoCond (blue curves) and Cond (red curves) runs at three redshifts. At $z = 1.4$, both simulations exhibit a classic cool-core (CC)

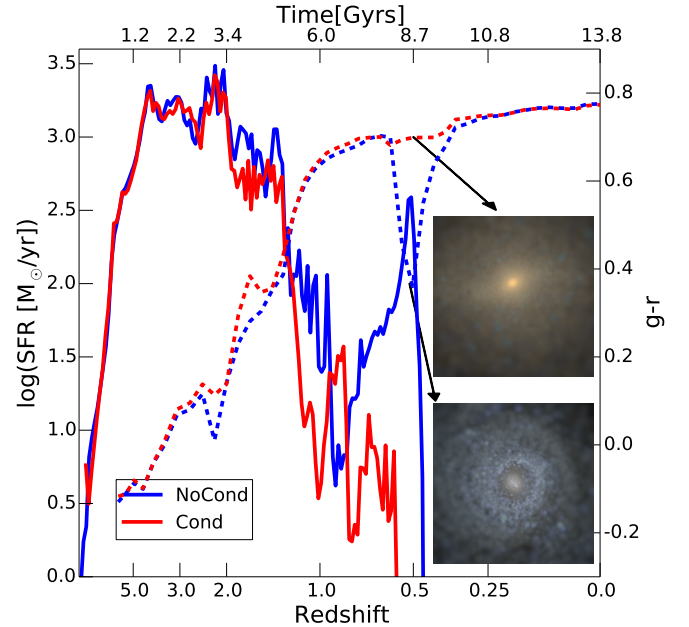


Figure 2. SFR (solid curves) and $g-r$ colors of the central galaxy (dashed curves) of the simulated cluster as a function of time for both the NoCond (blue curves) and Cond (red curves) runs. The insets show the synthetic SDSS g -, r -, and i -band composite images of the central galaxy of the cluster at $z = 0.5$.

structure, which is characterized by a temperature and entropy drop in the center and a central high density peak (Vikhlinin et al. 2006; Pratt et al. 2010). However, by $z = 0.7$, the Cond run has transitioned to a non-cool-core (NCC) cluster state, while the NoCond run still exhibits a CC structure. By $z = 0.35$, both the NoCond and Cond simulations show a NCC structure.

Another key difference is the lowering of the star formation rate (SFR) in the Cond run (Fig. 2) at low redshifts. Above $z \sim 2$, the SFRs (solid curves) of both the NoCond (blue curves) and Cond runs (red curves) are similar. After $z \sim 1.4$, when the transition from CC to NCC happens in the Cond run, a corresponding decrease in the SFR by almost a factor of three is seen.

At $z = 0.95$, the cluster starts undergoing a major ($\sim 1:1$) merger. The infall phase of the merger lasts for about 2 Gyrs, and the final coalescence of the central galaxies of the merging clusters takes place at about $z \sim 0.6$. This merger enhances the SFRs in both runs, but the amount of merger-induced star formation (SF) is drastically different in the two runs. The Cond run shows only a modest post-merger SFR of $\sim 10 M_{\odot}/\text{yr}$, while the NoCond run has SFRs that are as high as $300 M_{\odot}/\text{yr}$. Moreover, SF in the Cond run is completely quenched ~ 0.5 Gyrs before the NoCond run. We note that although the late time SFRs are very different in the two runs, the reduction in the total stellar mass in the Cond run is only about 10%. Furthermore, the stellar metallicities and the stellar ages of the central galaxy of the cluster are very similar in both runs. This is because most of the stellar mass has been built up before $z \sim 2$, where the SFRs are generally comparable since thermal conduction is not very effective at these times.

The discrepancy in the SFRs is also reflected in the intrinsic colors of the central galaxy (dashed curves and insets in Fig. 2), especially in the post merger phase of the cluster evo-

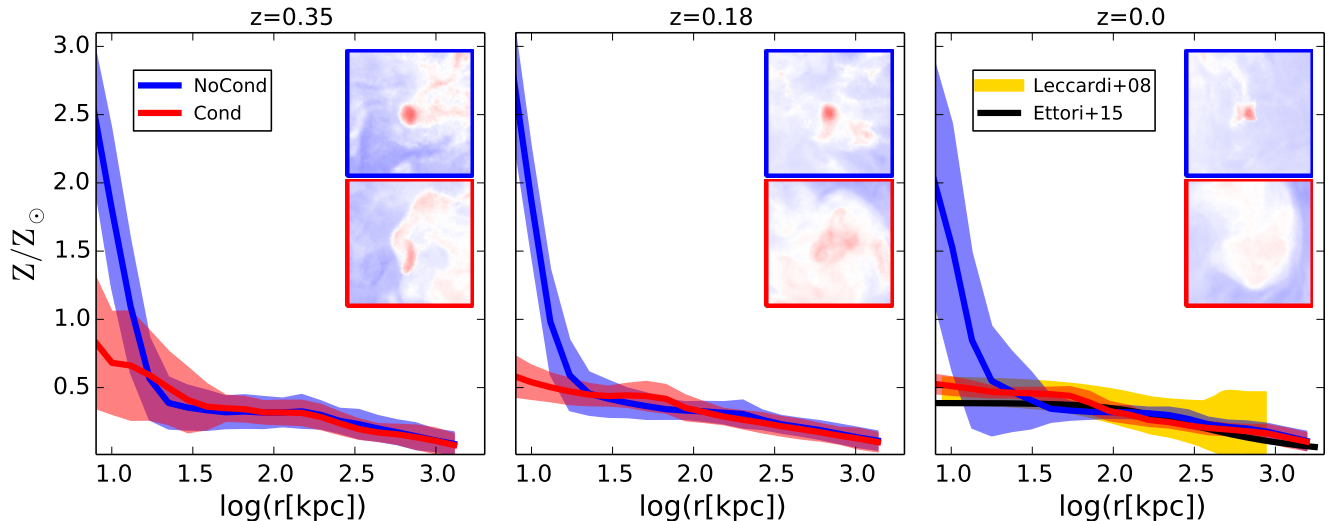


Figure 3. Gas metallicity profiles in the NoCond (red curves) and Cond (blue curves) runs at $z = 0.35$ (left column), $z = 0.18$ (middle column) and $z = 0.0$ (right column). The shaded regions denote the 1σ deviation from the mean. The insets in each panel show the projected mass-weighted gas metallicity maps in the NoCond (blue border) and Cond (red border) runs. The size of the projection box is $(200 \text{ kpc})^3$. The observational metallicity estimates at $z = 0$ from [Leccardi & Molendi \(2008\)](#) (yellow shaded region) and [Ettori et al. \(2015\)](#) (solid black curve) are overplotted.

lution. The $g-r$ color of the central galaxy in the Cond run is as high as ~ 0.8 , which places the galaxy in the red cloud, whereas the high SFRs in the NoCond run reduces the $g-r$ color to ~ 0.4 for about 2 Gyrs after the merger. Subsequently, AGN feedback turns the galaxy red again.

The right panel of Fig. 3 shows the gas metallicity profiles of the simulated clusters in the NoCond (blue curve) and Cond (red curve) runs at $z = 0$. The corresponding shaded regions denote the 1σ deviation from the mean metallicity. While the gas phase metallicities in the outer parts of the cluster are quite similar in both runs, the difference between them (in both the mean value and dispersion) within the core of the cluster ($r \leq 100 \text{ kpc}$) is quite striking. The Cond run reproduces observational estimates ([Leccardi & Molendi 2008](#); gold shaded region & [Ettori et al. 2015](#); solid black curve) of the metallicity profiles in clusters more faithfully.

The lower SFRs at $z < 1$ in the Cond run can in principle explain the low metallicity values in the center. However, this does not explain the lower dispersion of metallicities at a fixed radius. In order to understand this behavior, we plot mass-weighted gas metallicity maps and the corresponding profiles (Fig. 3) for both the NoCond and Cond runs. We chose $z = 0.35$ as our starting redshift because both runs have at that point a quenched galaxy in the center, and they have entered a relatively quiescent phase of evolution. There is no metal enrichment due to star formation and the only outflow mechanism is AGN driven winds. At $z = 0.35$, both the runs start out with a central metallicity core. The core in the NoCond run has a higher metallicity and is more concentrated because of the larger star formation rates at late times. However, by $z = 0$, the core in the Cond run is completely mixed, making the metallicity profile extremely flat and lowering its dispersion, while the core in the NoCond run still exists. These results point to the fact that conduction leads to significantly increased metal mixing, driven by turbulence injected by the central AGN.

4. DISCUSSION

We conclude that the inclusion of anisotropic thermal conduction has a strong effect on the properties of the ICM (i.e.,

temperature, entropy, density, metallicity profiles) and on the characteristics of the central galaxy (star formation rates, colors etc.). There are three possible mechanisms through which conduction can cause these changes. (1) Thermal conduction might force the AGN to inject more energy into the cluster core by conducting heat outwards, (2) conductive heating during the CC phase might offset cooling losses, or (3) thermal conduction might couple the injected AGN energy more efficiently with the ICM. Fig. 4 shows that the amount of energy deposited by the central AGN in the Cond run (solid red curve) is consistently lower than in the NoCond run (solid blue curve) by about 20–30%. This rules out the first mechanism.

Conductive heating in the CC phase of cluster evolution can in principle offset the cooling losses in the core, thereby reducing SF. However, this does not explain the suppression of SF when the Cond run shows a NCC structure. More importantly, throughout the CC phase of cluster evolution the conduction luminosity ($L_{\text{cond}} \sim -\kappa \partial T / \partial r$) in the Cond run is an order of magnitude lower than both the injected AGN luminosity and the total cooling luminosity within the cluster core. Consequently, we can safely conclude that conductive heating cannot be the full explanation for the observed differences between the two runs. It can provide at best a part of the energy needed in the CC phase.

Thus, a more efficient coupling of the injected AGN feedback energy with the surrounding ICM, mediated by conduction, seems to be the most plausible explanation. The AGN feedback model used in our simulations distinguishes between a high accretion rate quasar-mode feedback channel, modeled through local thermal energy injection, and a low accretion rate kinetic feedback mode, imparting momentum into the surrounding gas ([Weinberger et al. 2016](#)). The direction of the momentum injection is stochastic such that on average it is isotropic. The quasar mode feedback dominates at high redshifts, while the kinetic feedback mechanism becomes important below $z \sim 1.5$.

The metallicity evolution between $z = 0.35$ and $z = 0.0$ clearly demonstrates that there is more efficient turbulent mix-

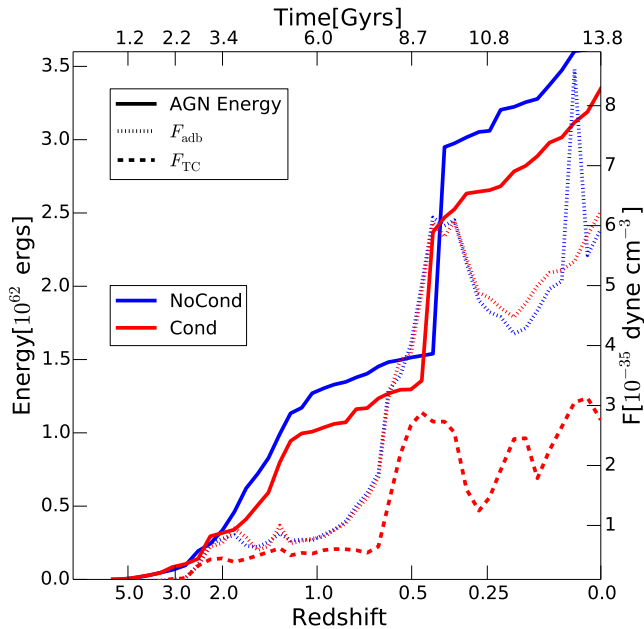


Figure 4. Cumulative amount of AGN energy injected into the ICM by the central blackhole (solid curves) in both the quasar and radio mode as a function of time. The mean value (within the central 100 kpc) of F_{adb} (dotted curves) and F_{TC} (dashed curve) is also plotted as a function of time. The blue curves denote the values obtained from the NoCond run, while the red curves show the values for the Cond run.

ing of the thermal plasma (and consequently metals) within the cluster core which can in principle explain the increased coupling efficiency between the AGN feedback energy and the ICM. However, the average (between $z = 0.35$ and $z = 0.0$) one-dimensional velocity dispersion profiles of the ICM (Fig. 5) in the NoCond (blue curve) run (150 km s^{-1}) is higher than in the Cond (red curve) run (100 km s^{-1}), especially in the cluster core. This seems to suggest that there is more metal/plasma mixing in-spite of lower turbulent velocities in the Cond run.

The ability of external turbulence to efficiently mix a stratified plasma depends on its convective stability, which, for a pure hydrodynamic plasma, is decided by its entropy gradient. Specifically, the plasma is stable as long as $\partial S/\partial r > 0$ (Schwarzschild criterion, Schwarzschild & Voigt 1992). This is generally true for all observed clusters (eg. Vikhlinin et al. 2006) and hence the ICM is conventionally thought to be convectively stable. In the presence of external turbulence, a fluid element in a stably stratified atmosphere which is adiabatically displaced from its equilibrium position by a small amount δr will experience a buoyant restoring force $F_{\text{adb}} \sim \rho g(d \ln S/dr) \delta r$ (Ruszkowski & Oh 2010), causing oscillations around its equilibrium position at the classical Brunt-Väisälä frequency. If the turbulent driving force (F_{turb}) is larger than the buoyant restoring force (F_{adb}) then it can induce mixing.

This picture changes in the presence of anisotropic thermal conduction because it fundamentally changes the response of the plasma to perturbations. Provided $dT/dr \neq 0$, conduction along magnetic field lines causes the ICM to be (formally) buoyantly unstable regardless of the temperature and entropy gradients. When $dT/dr > 0$ (for CCs in the central cooling region) the ICM is unstable to the heat-flux-driven buoyancy instability (Quataert 2008, HBI), and when $dT/dr < 0$ (for all clusters on large scales) it is unstable to the magneto-

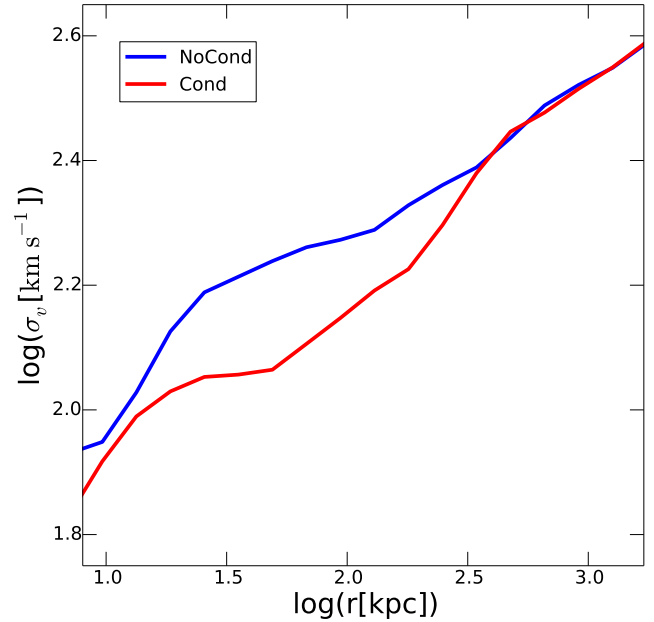


Figure 5. Average (between $z = 0.35$ and $z = 0$) one-dimensional velocity dispersion profiles in the NoCond (blue curve) and Cond (red curve) runs.

thermal instability (Balbus 2000, MTI). As a consequence, any amount of external turbulence will instantly mix the already convectively unstable (i.e., zero restoring force) thermal plasma without an energy penalty (Sharma et al. 2009). Even in the saturated state of these instabilities the buoyant restoring force is proportional to the temperature gradient ($F_{\text{TC}} \sim \rho g(d \ln T/dr) \delta r$) instead of the entropy gradient (Sharma et al. 2009).

Our blackhole feedback model is characterized by self-regulation, i.e. it keeps injecting energy until the cooling losses are accounted for. This implies that the AGN will essentially supply higher and higher turbulent energy until the injected turbulent driving force is larger than the buoyant restoring force, at which point it will induce mixing, isotropizing the injected energy and stopping cooling in the cluster core. The higher the buoyant restoring force, the larger the amount of turbulence injected by the AGN in order to induce mixing.

Fig. 4 shows that the restoring forces in the NoCond and Cond runs, calculated using the entropy gradient (F_{adb} , blue and red dotted curves, respectively), are quite similar. When we account for the fact that the buoyant response of an anisotropically conducting plasma is fundamentally different from that of a pure hydrodynamic fluid and calculate the restoring force using the temperature gradient (F_{TC} , red dashed line), we find lower restoring forces in the Cond run, which essentially explains the lower turbulent velocities and increased rate of plasma mixing in this run.

We note that F_{TC} is in principle only valid in the saturated state of the instabilities, otherwise the restoring forces are essentially zero. Hence, F_{TC} represents an upper limit to the restoring force in an anisotropically conducting plasma. It is very difficult to assess the state of these instabilities in fully cosmological simulations. We can however get some insights by noting that the timescale between successive AGN bursts, ~ 10 Myrs, is much smaller than the growth timescales for these instabilities, which is of the order of ~ 500 Myrs (Par-

ish et al. 2012). This implies that the HBI and MTI instabilities are unlikely to saturate or even grow considerably between successive AGN injection events. Besides, Fig. 5 clearly shows that it is not the additional turbulence generated by these instabilities that causes the plasma to mix, rather, they change the buoyant response of the ICM and make it more prone to mixing. It is the injection of turbulence into this modified state that causes the efficient mixing of the plasma. Therefore, the AGN kinetic wind power needed to induce gas mixing in the core is reduced. This allows the more efficient utilization of the injected energy in the Cond run, thereby drastically improving the coupling between the injected feedback energy and the ICM. The enhanced mixing of gas of different entropies will also contribute to a flattening of the entropy profiles in cool core phases of evolution.

Moreover, the increased mixing in the Cond run randomizes the magnetic field orientation, which in turn isotropizes the direction of conductive heat flow. This is particularly effective in redistributing the energy in the quasar mode of the AGN feedback, and in the high temperature regions (Weinberger et al. 2016) formed when the AGN kinetic winds shock against the ICM. Therefore, it seems that conduction enables turbulence, and turbulence enables conduction (Sharma et al. 2009; Ruszkowski & Oh 2010). Although we have shown that there is more mixing in the Cond run, we have not rigorously quantified this mechanism. This is beyond the scope of the current study and is left for future work.

5. CONCLUSIONS

We have presented cosmological MHD simulations of the formation of a galaxy cluster, comparing calculations with and without anisotropic thermal conduction. These are the first simulations to self-consistently include and quantify the effect of thermal conduction on both the integrated and small-scale properties of galaxy clusters. Our main results can be summarized as follows:

- Thermal conduction causes an earlier disruption of the cool core, and a subsequent reduction of the star formation rates by more than an order of magnitude at low redshift. The central gas phase metallicity gradients and dispersions are also reduced, despite an overall lower amount of AGN feedback energy injected into the ICM.
- The coupling between the AGN feedback energy and the ICM is effectively enhanced in the presence of anisotropic thermal conduction. It is considerably easier to mix thermal plasma in the presence of conduction, because the plasma is unstable irrespective of the temperature or entropy gradient and thus already prone to mixing. The restoring buoyancy forces are reduced, leading to efficient mixing even with low levels of external turbulent driving. This helps to isotropize the injected AGN feedback energy, thereby quenching the clusters more efficiently.

We have also simulated two other, less massive clusters ($M_{\text{halo}} \sim 2 \times 10^{14} M_{\odot}$ and $6 \times 10^{14} M_{\odot}$) at lower resolution. The general trends (earlier termination of the cool core, lower SFRs, and lower central metallicities and dispersion etc.) are very similar for these clusters, suggesting that our conclusions robustly apply to other systems as well.

We stress that although thermal conduction helps in quenching star formation, it is not sufficient on its own for stabilizing clusters or converting a cool core to a non cool core (at least not for these cluster masses). It only amplifies

the effect of external turbulent driving. The external source of turbulence can in principle take many forms, such as mergers, cosmic ray driven convection, etc., and is not limited to the kinetic AGN winds examined here. We thus expect that the importance of anisotropic thermal conduction carries over to other forms of feedback as well.

We thank Eliot Quataert for useful comments and discussions. MV acknowledges support through an MIT RSC award and the Alfred P. Sloan Foundation. RW, VS and RP acknowledge support by the European Research Council under ERC-StG grant EXAGAL 308037. CP acknowledges support by the European Research Council under ERC-CoG grant CRAGSMAN-646955. CP, RW, VS and RP also acknowledge support from the Klaus Tschira Foundation.

REFERENCES

- Angulo, R. E., Springel, V., White, S. D. M., et al. 2012, *MNRAS*, 426, 2046
- Balbus, S. A. 2000, *ApJ*, 534, 420
- Banerjee, N., & Sharma, P. 2014, *MNRAS*, 443, 687
- Booth, C. M., & Schaye, J. 2009, *MNRAS*, 398, 53
- Carilli, C. L., & Taylor, G. B. 2002, *ARA&A*, 40, 319
- Choi, E., Ostriker, J. P., Naab, T., & Johansson, P. H. 2012, *ApJ*, 754, 125
- Croton, D. J., Springel, V., White, S. D. M., et al. 2006, *MNRAS*, 365, 11
- Ettori, S., Baldi, A., Balestra, I., et al. 2015, *A&A*, 578, A46
- Genel, S., Vogelsberger, M., Springel, V., et al. 2014, *MNRAS*, 445, 175
- Hahn, O., Martizzi, D., Wu, H.-Y., et al. 2015, *ArXiv e-prints*, [arXiv:1509.04289](https://arxiv.org/abs/1509.04289)
- Hinshaw, G., Larson, D., Komatsu, E., et al. 2013, *ApJS*, 208, 19
- Kannan, R., Springel, V., Pakmor, R., Marinacci, F., & Vogelsberger, M. 2016, *MNRAS*, 458, 410
- Komarov, S. V., Churazov, E. M., Kunz, M. W., & Schekochihin, A. A. 2016, *MNRAS*, 460, 467
- Leccardi, A., & Molendi, S. 2008, *A&A*, 487, 461
- Li, Y., & Bryan, G. L. 2014, *ApJ*, 789, 54
- Pakmor, R., & Springel, V. 2013, *MNRAS*, 432, 176
- Parrish, I. J., McCourt, M., Quataert, E., & Sharma, P. 2012, *MNRAS*, 419, L29
- Pratt, G. W., Arnaud, M., Piffaretti, R., et al. 2010, *A&A*, 511, A85
- Quataert, E. 2008, *ApJ*, 673, 758
- Rasia, E., Borgani, S., Murante, G., et al. 2015, *ApJ*, 813, L17
- Riquelme, M. A., Quataert, E., & Verscharen, D. 2016, *ApJ*, 824, 123
- Roberg-Clark, G. T., Drake, J. F., Reynolds, C. S., & Swisdak, M. 2016, *ApJ*, 830, L9
- Ruszkowski, M., Lee, D., Brüggem, M., Parrish, I., & Oh, S. P. 2011, *ApJ*, 740, 81
- Ruszkowski, M., & Oh, S. P. 2010, *ApJ*, 713, 1332
- Schaye, J., Crain, R. A., Bower, R. G., et al. 2015, *MNRAS*, 446, 521
- Schwarzschild, K., & Voigt, H.-H. 1992, *Gesammelte Werke / Collected Works*
- Sharma, P., Chandran, B. D. G., Quataert, E., & Parrish, I. J. 2009, *ApJ*, 699, 348
- Sijacki, D., Springel, V., Di Matteo, T., & Hernquist, L. 2007, *MNRAS*, 380, 877
- Sijacki, D., Vogelsberger, M., Genel, S., et al. 2015, *MNRAS*, 452, 575
- Spitzer, L. 1962, *Physics of Fully Ionized Gases*
- Springel, V. 2010, *MNRAS*, 401, 791
- Springel, V., & Hernquist, L. 2003, *MNRAS*, 339, 289
- Vikhlinin, A., Kravtsov, A., Forman, W., et al. 2006, *ApJ*, 640, 691
- Vogelsberger, M., Genel, S., Sijacki, D., et al. 2013, *MNRAS*, 436, 3031
- Vogelsberger, M., Sijacki, D., Kereš, D., Springel, V., & Hernquist, L. 2012, *MNRAS*, 425, 3024
- Vogelsberger, M., Genel, S., Springel, V., et al. 2014a, *MNRAS*, 444, 1518
- . 2014b, *Nature*, 509, 177
- Voit, G. M., Donahue, M., Bryan, G. L., & McDonald, M. 2015, *Nature*, 519, 203
- Weinberger, R., Springel, V., Hernquist, L., et al. 2016, *ArXiv e-prints*, [arXiv:1607.03486](https://arxiv.org/abs/1607.03486)
- Yang, H.-Y. K., & Reynolds, C. S. 2016, *ApJ*, 818, 181
- Zakamska, N. L., & Narayan, R. 2003, *ApJ*, 582, 162